Comparative study of PtNi nanowire array electrodes toward oxygen reduction reaction by half-cell measurement and PEMFC test

Mardle, Peter; Thirunavukkarasu, Gnanavel; Guan, Shaoliang; Chiu, Yu-Lung; Du, Shangfeng

DOI:
10.1021/acsami.0c11531

Document Version
Peer reviewed version

Citation for published version (Harvard):
Mardle, P, Thirunavukkarasu, G, Guan, S, Chiu, Y-L & Du, S 2020, 'Comparative study of PtNi nanowire array electrodes toward oxygen reduction reaction by half-cell measurement and PEMFC test', *ACS Applied Materials & Interfaces*, vol. 12, no. 38, pp. 42832–42841. https://doi.org/10.1021/acsami.0c11531

Comparative study of PtNi nanowire array electrodes toward oxygen reduction reaction by half-cell measurement and PEMFC test

Peter Mardle[1†], Gnanavel Thirunavukkarasu[2], Shaoliang Guan[3,4], Yu-Lung Chiu[2] and Shangfeng Du[1]*

1. School of Chemical Engineering, University of Birmingham, Edgbaston, Birmingham, B15 2TT, UK

2. School of Metallurgy and Materials, University of Birmingham, Edgbaston, Birmingham, B15 2TT, UK

3. School of Chemistry, Cardiff University, Cardiff, CF10 3AT, UK

4. HarwellXPS - The EPSRC National Facility for Photoelectron Spectroscopy, Research Complex at Harwell (RCaH), Didcot, Oxon, OX11 0FA, UK

[*]Corresponding author, Tel: +44 121 4158696

E-mail address: s.du@bham.ac.uk (S. Du)

Keywords: Proton exchange membrane fuel cell (PEMFC), gas diffusion electrode (GDE), PtNi, nanowire, ionomer

Abstract

A clear understanding of catalytic activity enhancement mechanisms in fuel cell operation is necessary for a full degree translation of the latest generation of non-Pt/C fuel cell electrocatalysts into high performance electrodes in proton exchange membrane fuel cells (PEMFCs). In this work, PtNi nanowire (NW) array gas diffusion electrodes (GDEs) are fabricated from Pt nanowire arrays with Ni impregnation. A 2.84-fold improvement in the ORR catalytic activity is observed for the PtNi NW array GDE (*cf*. the Pt NW array GDE) using half-cell GDE measurement in 0.1 M $HClO_4$ aqueous electrolyte at 25°C, in comparison to only 1.07-fold power density recorded in PEMFC single cell test. Ionomer is shown to significantly increase electrochemically active surface area of the GDEs, but the PtNi NW array GDE suffers from Ni ion contamination at a high temperature, contributing to decreased catalytic activities and limited improvement in operating PEMFCs.

1. Introduction

The proton exchange membrane fuel cell (PEMFC) is a key technology in the development of environmentally friendly and sustainable hydrogen based energy economies. The widespread adoption of this technology is limited by the high cost of the Pt based catalysts, representing up to 40% of the total fuel cell cost [1]. Significant reduction in the platinum group metal (PGM) loading was made in 1980s by the development of the currently common used catalyst layer (CL) made of Pt nanoparticles supported on carbon (Pt/C) mixed with proton conducting ionomer [2]. Afterwards, research has focused on improving inherent catalytic activities of Pt based catalysts towards the oxygen reduction reaction (ORR) in order to ultimately reduce the amount required in PEMFC systems [3,4]. Great advancements have been made in both understanding the compositional and structural attributes that make the ideal ORR catalyst [5], and nanomaterial synthesis techniques, culminating in catalysts with a mass activity of 30 times higher than that defined in the DoE 2020 targets [6].

Despite this, the catalyst loading at the cathode in practical fuel cell applications is still around 0.2 mg_{Pt} cm^{-2}, corresponding to a reduction of just half of those three decades ago. One factor for the low performance in fuel cells is the dependence of local O_2 transport resistance on the roughness factor of PEMFC electrodes whereby a low loading is disadvantaged at a high current density [7], in addition to the limitations imposed by virtue of Butler-Volmer kinetics [8]. There has also been a clear disparity reported between the catalytic performance of non-Pt/C ORR catalysts demonstrated in half-cell electrochemical measurement in liquid electrolytes (usually using the rotating disk electrode (RDE) technique) and those obtained in a working PEMFC [9–11]. In this critical time of climate change, it is crucial for this disparity to be better understood and for material scientists to focus on the translation of the high activities of the latest generation of fuel cell

catalysts into higher performance PEMFCs, therefore facilitating this clean technology for an extensive commercialization.

One branch of non-Pt/C catalysts that have shown both promising ORR catalytic activities and PEMFC performance is one-dimensional (1D) nanostructures such as Pt nanowires (NWs) [6,12]. Due to their highly ordered crystalline structure, enhanced specific activities of 1D nanostructures over 0D nanoparticle (NP) analogues have been demonstrated [13–15]. NWs have also been shown to be more stable than NPs due to a reduced susceptibility to surface dissolution, aggregation and Ostwald ripening [16]. Of particular interest is the simple, surfactant and template free formic acid reduction method to synthesize ultra-thin single crystal Pt NWs grown along the <111> crystal direction [17]. Sun et al synthesized unsupported and supported Pt NW catalysts using this method and demonstrated improved ORR activities and stability [18,19]. Our group has since adapted this formic acid reduction approach for the highly simple fabrication of gas diffusion electrodes (GDEs) with Pt NW arrays. Initially, Pt NWs were grown on carbon paper gas diffusion layers (GDLs) where outstanding ORR activity was observed by improved O_2 mass transport properties, as a direct result of the high aspect ratio of NWs obtained in addition to the thin CL structure [20]. Iterations on this work have demonstrated improved NW distribution through the modification of the GDL surface such as by using Pd nanoseeds [21,22], active screen plasma (ASP) nitriding [23] or the refinement of reaction temperature [24], all of which demonstrated improved fuel cell performance.

Inspired by promising catalytic activities of PtNi alloys, a method of fabricating PtNi NWs via the post-synthetic reduction and annealing of Ni onto the Pt NW structure was demonstrated on carbon nanosphere support [25]. With this simple process, the mass activity of the Pt NW/C catalyst was boosted by 1.78-fold (using half-cell electrochemical measurement in liquid electrolyte). However, the single cell test in PEMFCs showed very poor power performance as a consequence

of surface Ni hydroxide species. Here, this method of Ni incorporation onto pre-existing Pt structures is combined with post acid leaching treatment for fabricating PtNi NW array GDEs. The annealing temperature, ionomer content and acid leaching are studied to understand the influence mechanisms of the catalyst surface properties with the GDEs based on the power density recorded in PEMFC test and intrinsic catalytic activities obtained using ex-situ GDE measurement in liquid electrolyte. It is expected the knowledge achieved here could provide a better understanding of the disparity between half-cell electrochemical measurement and PEMFC tests in the evaluation of the catalytic performance of PtM alloys.

2. Experimental

2.1. Materials

All H_2O used was deionised using a Millipore water system (18 MΩ). Sigracet 39BC carbon paper was used as GDLs. H_2PtCl_6 (8 wt% in H_2O), HCOOH (≥ 95%), isopropyl alcohol (IPA), $NiCl_2.6H_2O$, $NaBH_4$ and HCl (37%) were purchased from Sigma-Aldrich. HNO_3 (70%) was obtained from Fisher Chemicals. 0.1 M NaOH was made in-house with 10 M NaOH solution from Fluka Biochemika. 10% Nafion® solution (D1021) was purchased from Ion Power Inc. Pt/C catalyst (45.9 wt_{Pt}%, TEC10E50E) from Tanaka KikinzokuKogyo K. K. (TKK) was used as a benchmark and Johnson Matthey (JM) 0.4 mg_{Pt} cm^{-2} GDEs were used as anodes for the preparation of membrane electrode assemblies (MEAs).

2.2. PtNi NW array GDE fabrication

Pt NW array GDEs were fabricated using a slightly modified procedure to that detailed previously [24]. A 100 cm^2 Sigracet 39BC GDL was placed at the bottom of an equal sized petri-dish

and submerged in 66 mL H_2O. 1.05 mL of 8 wt% H_2PtCl_6 aqueous solution was added, followed by 3.31 mL HCOOH. The petri dish was covered by the lid and placed in an oven at 40°C for 72 hrs. The Pt NW array GDE was then washed with H_2O and IPA before drying in the oven at the same temperature.

Ni impregnation was conducted at a precursor ratio equivalent to Pt_3Ni_4. A 16 cm^2 square cut from the as-prepared Pt NW array GDE was painted with a solution of 10.4 mg $NiCl_2.6H_2O$ in 100 µL H_2O before pipetting a fresh solution of 10.4 mg $NaBH_4$ in 1 mL NaOH solution (0.1 M). This was left to react for 2 hrs before washing and drying.

Thermal annealing was carried out in a tube furnace (Vecstar Ltd) at the select temperature (150, 200 or 250°C) for 24 hrs under a 50 mL min^{-1} flow of 4% H_2/Ar. The heating and cooling rate was 2°C min^{-1}. Acid leaching (AL) was performed by submerging the annealed GDE in 0.1 M HNO_3 solution for 2 hrs. The entire PtNi NW array GDE fabrication process is shown in Figure 1.

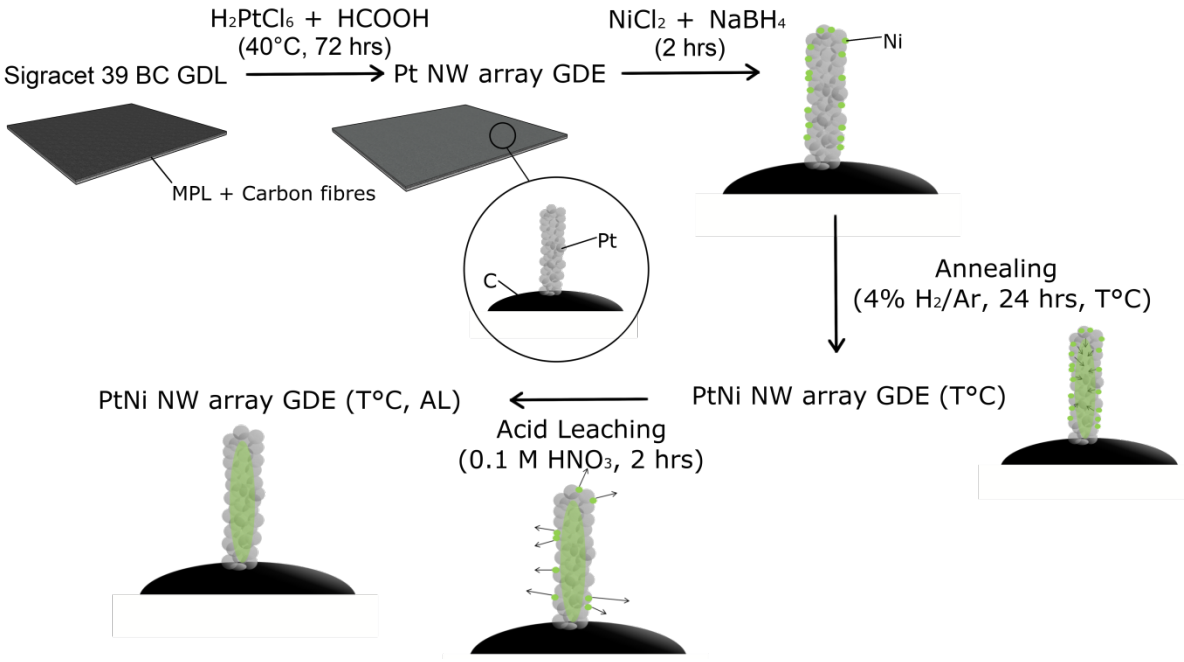

Figure 1. Schematic fabrication process of the PtNi NW array GDE (T°C represents the annealing temperature).

2.3. Physical characterisation

Scanning electron microscopy (SEM) analysis was conducted on a Jeol 7000F SEM. A TM3030Plus SEM was used for the cross-sectional analysis and energy dispersive X-ray (EDX) mapping. A Thermo Scientific™ Talos F200X (S)TEM with an accelerating voltage 200 kV was used for all transmission electron microscopy (TEM) and scanning transmission electron microscopy (STEM) analysis. Inductively coupled plasma mass spectrometry (ICP-MS) was conducted on both entire GDEs (1 cm^2) and the CL (0.5 - 1 mg scrapped off) by a Perkin Elmer Nexion 300X with plasma strength 1500 W. X-ray diffraction (XRD) analysis was carried out with a Bruker D8 auto-sampler using a Cu X-ray source (λ = 0.15406 nm) with a step size of 0.02°. A Thermo Fisher Scientific NEXSA spectrometer with a micro-fused monochromatic Al Kα source (72 W) and a spot size 300 x 300 μm was used for X-ray photoelectron spectroscopy (XPS) of the GDE surface. Data analysis was performed with the Casa XPS software (version 2.3.18PR1.0) and sample charge corrected using the C1s peak at 284.8 eV as the reference point.

2.4. Ex-situ GDE measurement

Ex-situ GDE measurement was conducted in a 3-electrode setup using a FlexCell (PTFE) from Gaskatel. GDEs were cut to 5 cm by 3 cm rectangular pieces for measuring. The GDE was held in the cell by O-rings with an active area of 3 cm^2 and used as the working electrode. The main and reference compartments were filled with 0.1 M $HClO_4$ aqueous electrolyte. A commercial HydroFlex reference hydrogen electrode (RHE) was used and Pt coil was used as the counter

electrode. The cell temperature was kept at 25°C. A cross sectional Illustration of the measurement apparatus is shown in Figure 2.

Initially with N_2 gas supplied behind the GDE, 100 cycle voltammetry (CV) cycles were conducted in the range 0.05-1.2 V vs. RHE at 100 mV s^{-1} in order to electrochemically clean the catalyst surface. 2 CVs were then recorded at 20 mV s^{-1} with the last used for Pt surface area calculation. The gas was then switched to O_2 and the open circuit potential (OCP) was recorded until it became stable for at least 200 s as an indication of saturation. A linear sweep voltammogram (LSV) was then run from 1.2 - 0.05 V vs. RHE at 10 mV s^{-1} and potentio-electrochemical impedance spectroscopy ((P)EIS) was conducted at 0.9 V vs. RHE in the frequency range of 10 kHz - 0.1 Hz.

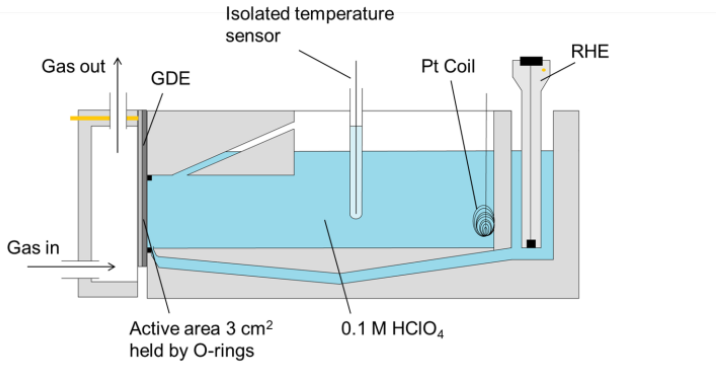

Figure 2: Cross sectional Illustration of the FlexCell (PTFE) ex-situ GDE measurement apparatus.

2.5. MEA fabrication and single cell testing

The MEA fabrication and testing procedures were detailed in our previous work [26]. Typically, Nafion® ionomer was coated onto the 16 cm^2 GDEs (91.4 µL 10% Nafion® solution in 200 µL IPA, for an ionomer loading of 0.6 mg_{Nafion} cm^{-2}) before being made into MEAs. The test cathode and commercial anode were hot pressed at both side of a Nafion® 212 membrane (36 cm^2) under a load of 1800 lb at 135°C for 2 mins.

A PaxiTech-Biologic FCT-50S PEMFC test stand was used for all MEA tests. Polytetrafluoroethylene (PTFE) gasket of thickness 254 μm and graphite flow field plates with single serpentine channels are used. For all tests the cell temperature was 80°C. Membrane hydration was firstly achieved by holding the cell potential at 0.6 V for more than 10 hrs with air/H_2 supplied at stoichiometric ratios of 1.5/1.3 control under 1.5/1.5 bar absolute pressure and 100/100% relative humidity (RH), respectively. Polarization curves were obtained following the EU harmonised test protocol, and the cathode/anode conditions were changed to 2.3/2.5 bar absolute pressure and 30/50% RH, respectively [27]. Under these conditions (G)EIS (30 mA cm^{-2} with an amplitude of 4.5 mA cm^{-2}) and (P)EIS (0.65 and 0.5 V with an amplitude 10 mV) were conducted in the frequency range 10 kHz - 0.1 Hz. Kinetic characterisation was conducted under U.S. department of energy (DoE) standard protocol with the cathode/anode supplied with O_2/H_2 at 9.5/2 stoichiometric ratio at 1.5/1.5 bar absolute pressure and 100/100% RH, respectively [28]. An EZ-Stat Pro (NuVant Systems) was used to record cathode CVs (0.05 - 1.2 V vs. RHE at 20 mV s^{-1}) as well as measure H_2 crossover current by holding the potential at 0.5 V vs. RHE for 30 mins [29]. For these tests the cathode was fed with fully humidified N_2. The $H_{desorption}$ region of the CV plot and the capacitive constant of 210 μC cm^{-2} for polycrystalline Pt was used to calculate the electrochemical surface area (ECSA) [30]. Accelerated degradation testing (ADT) was conducted by performing 3000 potential sweep cycles in the potential range of 0.6 - 1.2 V vs. RHE at 100 mV s^{-1} to monitor the GDE durability in PEMFCs.

3. Results and Discussion

3.1. Physical characterisation

SEM analysis results of the PtNi NW array GDE (annealed at 200°C) are shown in Figure 3. The NWs show some cubic agglomerate structures with NWs just visibly protruding out from the surface (Figure 3a). Additionally, NWs tend to form clusters which as approximated by SEM-EDX, showing a 2-3 fold increase in Pt density as compared to the rest of the GDL surface (Figure S1). Figure 3b-3d shows the cross-section SEM image and Ni EDX mappings of the GDEs with and without acid leaching (AL). For the one before AL, a band of Ni is clearly visible at the interface between carbon fibre substrate and microporous layer (MPL) in the GDE (Figure 3c). In the impregnation step, the Pt NW array GDE is wetted but the highly hydrophobic fibrous carbon substrate still contains numerous air pockets. Most $NiCl_2.6H_2O$ precursor resides at this interface forming Ni particles on location by a following reduction process using $NaBH_4$. Rather than $NaBH_4$, hydrazine monohydrate has alternatively been used by Elvington et al, however, there is no evidence that this would more preferentially reduce Ni on the NW surface [31]. The Ni band is effectively removed in the following acid leaching procedure and leaving behind a high Ni content on the surface with the CL in the GDE (Figure 3d). Clear evidence of the Ni content decrease is demonstrated with the ICP-MS results presented later.

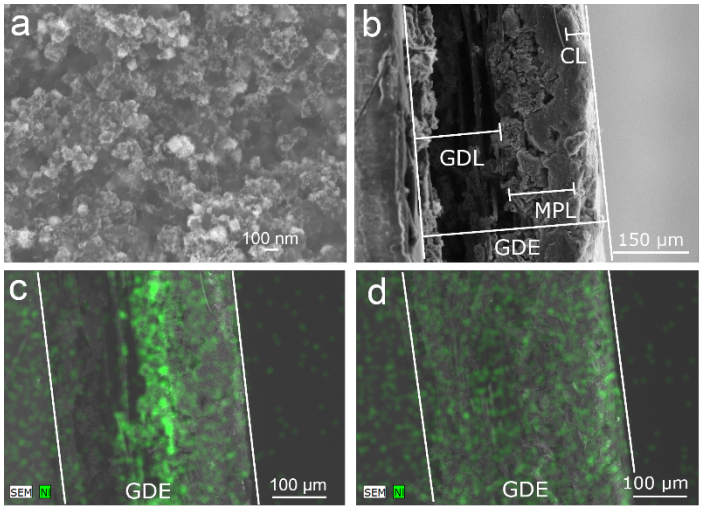

Figure 3: SEM analysis of a PtNi NW array GDE after annealing at 200°C: **(a)** surface image; and **(b)** the cross-section image after the acid leaching (AL). SEM-EDX Ni mappings of the PtNi NW array GDE annealed at 200°C **(c)** before and **(d)** after the acid leaching. White lines indicate the cross-section area.

TEM images of the PtNi NW arrays illustrate the cubic agglomerates with an average size of about 120 nm as comprised of NWs of lengths about 25 nm (Figure 4), consistent with previous reports [24]. This agglomerate structure has been frequently reported in previous works on this fabrication method where it is thought that a highly crystalline seed provides the facets for the orientated growth of the NWs [19,32]. The average diameter of the NWs is about 3.9 nm with little change across the three different annealing temperatures investigated (Figure 4b-d). Lattice fringe patterns (Figure 4e) indicate an average inter lattice spacing of 0.22 nm, confirming anisotropic growth along the <111> direction. STEM-EDX mapping was also employed to confirm the incorporation of Ni into the Pt NW structure through impregnation and annealing (Figure 4f-g).

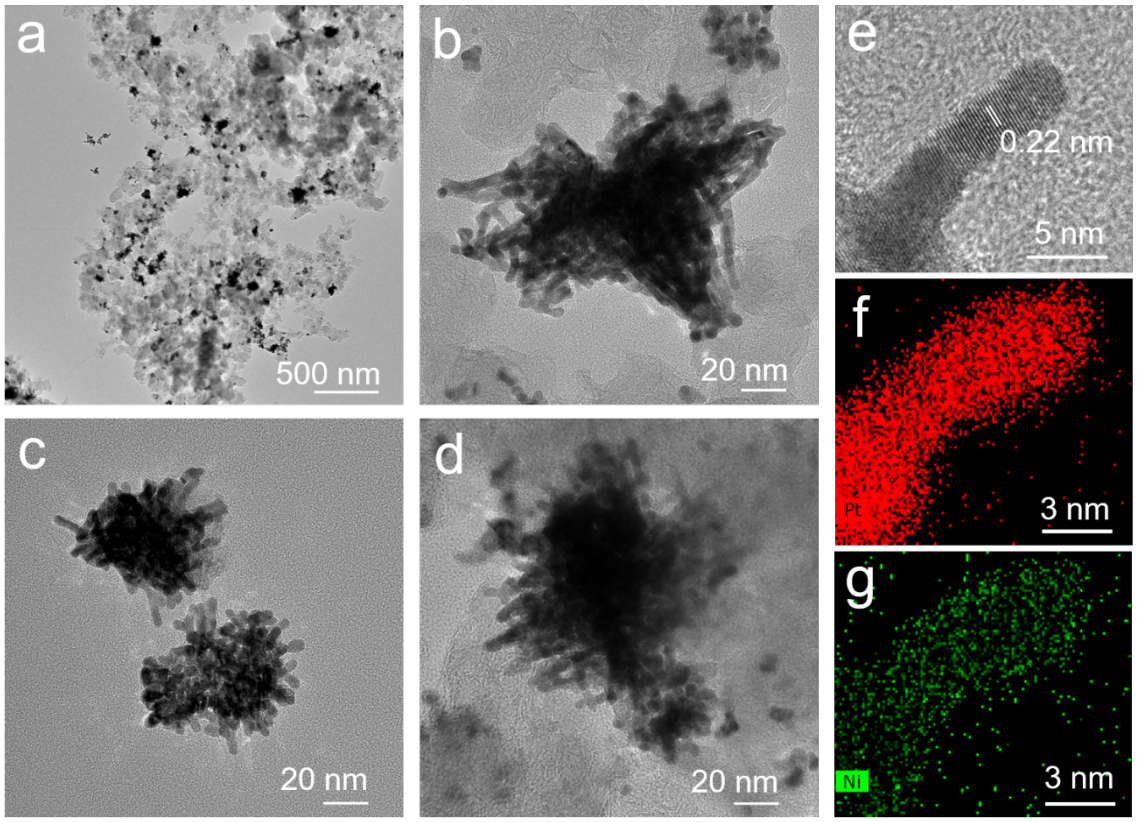

Figure 4: TEM of PtNi NW arrays acid leached after annealing for 24 hrs at the temperatures of **(a)** and **(b)** 200, **(c)** 150 and **(d)** 250°C. **(e)** HR-TEM showing the inter lattice spacing of a PtNi NW (150°C). **(f)** Pt and **(g)** Ni STEM-EDX maps of a PtNi NW (200°C, AL).

ICP-MS analysis was used to accurately determine the Pt-Ni ratio for the entire GDE and the CL of the PtNi NW array GDEs to further understand Ni impregnation. This was conducted to the GDEs (fabricated with a precursor ratio of Pt_3Ni_4) with three different annealing temperatures before and after the acid leaching. Figure 5a shows the obtained Pt_xNi ratios. An average value of x = 1.11 is obtained for the entire GDE before the acid leaching, representing a yield of 67% for the Ni reduction where the rest is washed away during the GDE cleaning procedure. After the acid leaching, x = 4.55, suggesting removal of 76% Ni. For the CL, x is 4.59 and 4.34 before and after the acid leaching, respectively. These values lead to two main conclusions: (i) The Ni incorporated

into the CL is stable under the acid leaching conditions employed in this study, suggesting the successful surface segregation of Pt during the annealing process for a good protection of the annealed Ni. (ii) The Ni content of the entire GDE after the acid leaching is very close to that of the CL - where the ratio is much smaller for the entire GDE before the acid leaching. In conjunction with the SEM-EDX results shown in Figure 3c and 3d, this suggests that the acid leaching mainly removes the Ni in the carbon paper/MPL interface which can potentially hinder MEA performance, but retains the part within the NWs that can boost ORR catalytic activities. A detailed investigation of the optimal acid leaching conditions similar to the work conducted by Alia et al [33] will be of interest to this electrode system, however this is beyond the scope of this study. In addition to the determination of the Pt_xNi ratio, ICP-MS was also used to ascertain the average Pt loading. A value of 0.312±0.026 mg_{Pt} cm^{-2} is obtained and is taken as the catalyst loading for all NW GDEs herein.

XRD analysis was conducted to understand the crystallinity and the alloying degree of the PtNi NWs within the GDEs. Figure 5b shows the XRD patterns of the Pt/C, Pt NW array and PtNi NW array (200°C, AL) GDEs. The high C peak at 26.6° is associated with the (002) plane of the graphitic carbon with the GDL support. All other peaks can be well indexed to the face centred cubic (fcc) Pt structure (JCPDS-04-0802) [34]. With the NW arrays a high degree of crystallinity of Pt results in much larger peak intensity than Pt/C. Figure 5c shows Pt (111) peaks for the Pt NW array and PtNi NW array GDEs annealed at the different temperatures, including those that have undergone acid leaching. A progressive positive peak shift can be observed with the increase of the annealing temperature, indicating lattice contraction through the surface segregation of Pt and alloying of the smaller Ni atoms into the Pt fcc lattice, coinciding with our previous study [25]. This peak shift is lower than those of PtNi alloy nanostructures reported in literature due to the low

annealing temperature used here for retaining NW morphology and the low Ni content in the final NW structures [31,35,36]. Pt(111) peaks for the PtNi NWs before and after the acid leaching (dotted) were observed to be very similar, further demonstrating the stable incorporation of Ni in the Pt NWs.

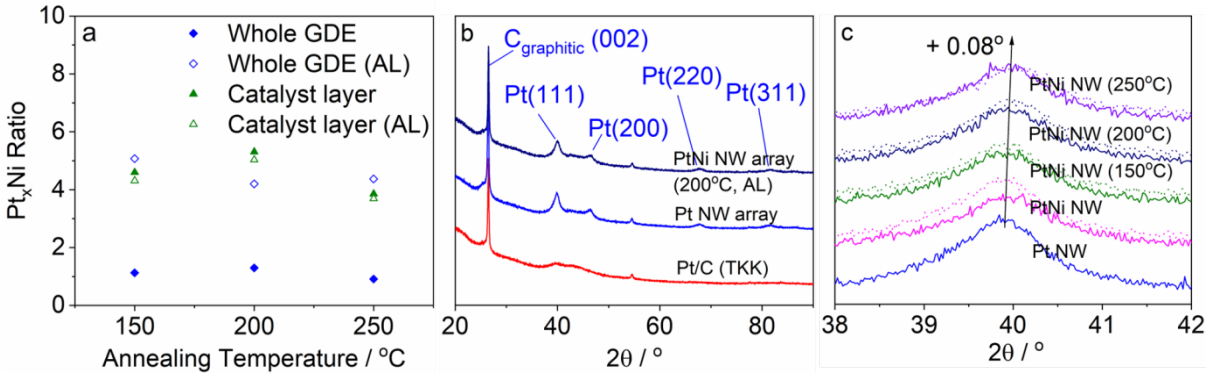

Figure 5: (a) Pt$_x$Ni ratios for the PtNi NW array GDEs and CLs annealed at three different temperatures before and after the acid leaching (AL). The values of x are presented on the vertical axis. **(b)** XRD patterns of the GDEs made of Pt/C, Pt NW arrays and PtNi NW arrays (200°C, AL). **(c)** Comparison of Pt (111) peak for the Pt NW and PtNi NW array GDEs annealed at different temperatures and after acid leaching (dotted).

XPS analysis was employed to evaluate the nature of Pt and Ni elements in the GDEs. Figure 6a shows the survey spectra of the Pt NW array and PtNi NW array (200°C) before and after the acid leaching. The peak at around 1072 eV for the PtNi NW array GDE before the acid leaching is Na 1s (Figure S3), resourcing from $NaBH_4$ reductant, which has an adverse effect on PEMFC performance through cation exchange, similar to dissolved Ni ions [37]. Fitting of the Pt 4f spectra shows just metallic Pt across all GDEs indicating a high stability of Pt to oxidation by the HNO_3 used in the acid leaching (Figure 6b-c). In addition to the Pt peaks, Ni 3p peaks can be observed and increase after the acid leaching, in particular at the low annealing temperature of 150°C (Figure S4). Ni 2p XPS shows that the ratio of Ni/Ni oxides decreases after the acid leaching for the PtNi

NWs suggesting oxidation by the acid (Figure 6d-f). This Ni/Ni oxide ratio increases with the annealing temperature indicating improved protection of the subsurface Ni to oxidation, while unprotected Ni oxides on the surface are completely removed during the acid leaching process. Alia et al commented that when forming a Ni oxide layer on the PtNi NWs by thermal annealing in O_2, Ni oxide could segregate to the surface under certain conditions (e.g. annealing at 300°C) leading to very little Pt presented on the surface [38]. The greater intensity of Ni 3p peaks in the Pt 4f spectra after acid leaching implies that the oxidation of Ni from acid leaching also induces the surface segregation of Ni back to the surface layers of the PtNi NWs. A high annealing temperature results in a more stable alloy which can partially prevent this segregation.

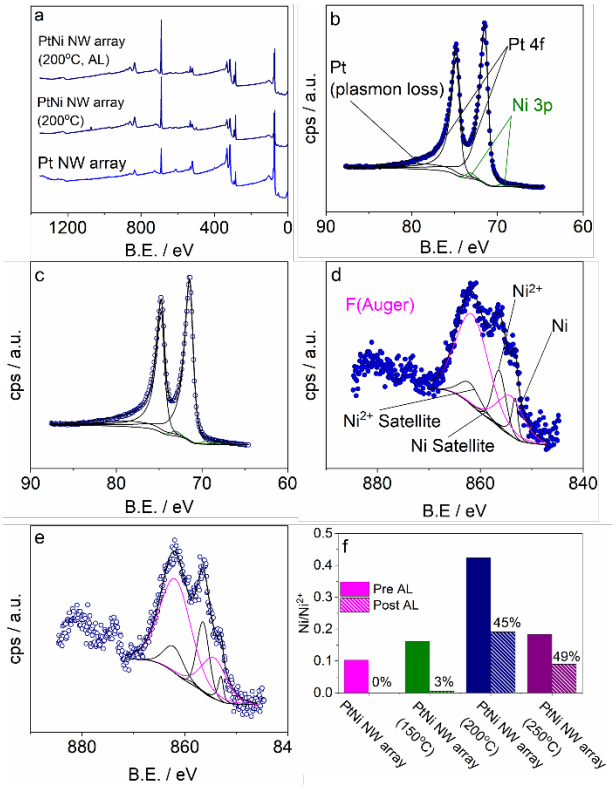

Figure 6: (a) Survey XPS spectra for the Pt NW array and PtNi NW array GDEs annealed at 200°C before and after the acid leaching. Pt 4f XPS spectra of **(b)** PtNi NW array (200°C) and **(c)**

PtNi NW array (200°C, AL). Ni 2p XPS spectra for **(d)** PtNi NW array (200°C) and **(e)** PtNi NW array (200°C, AL). **(f)** Ni/Ni oxide ratios for all PtNi NW GDEs based on the peak area.

3.2. Ex-situ GDE measurement

The environment in operating fuel cells is very complex depending on many different factors rather than just the catalysts themselves. For example, Ni leached out of the NWs can contaminate the local ionomer, which thus decreases the local O_2 permeability and proton conductivity at the catalyst surface. To evaluate the impact of Ni impregnation on the catalytic activity in a clean environment by mitigating influence of external circumstances, ex-situ GDE measurement was conducted to the Pt NW array and PtNi NW array (200°C, AL) GDEs in 0.1 M $HClO_4$ aqueous electrolyte. Both Pt NW array and PtNi NW array GDEs with and without the inclusion of Nafion® ionomer were measured and the results are shown in Figure 7. The CV plots (Figure 7a) show that without ionomer, natural hydrophobicity of the GDL limits the wettability of the liquid electrolyte and very low ECSAs of 4.2 and 5.5 $m^2 g_{Pt}^{-1}$ are obtained for Pt NW array for PtNi NW array GDEs, respectively. When ionomer is loaded onto the GDEs, the ECSAs increase to 26.8 and 29.0 $m^2 g_{Pt}^{-1}$, respectively.

After the CV scanning the electrolyte solution was saturated with O_2 gas, where OCP was used as a measure of saturation, and the cathodic LSV was then recorded (Figure 7b-c). The mass activities at 0.9 V vs. RHE for all plain and ionomer coated GDEs are listed in Table S1 and compared in Figure 7d. The mass activities for the plain Pt NW array and PtNi NW array GDEs are 0.83 and 3.39 mA mg_{Pt}^{-1}, and these increase to 5.08 and 14.44 mA mg_{Pt}^{-1} after coating with ionomer. The large increase is as expected because the ionomer boosts the contact between the electrolyte with the NW surface. The much enhanced activity of the PtNi NW array GDE in comparison to the Pt NW array GDE (4.08- and 2.84-fold without and with ionomer, respectively)

confirming the positive role of Ni in boosting the inherent catalytic activity of the NWs, but the large decrease from 4.08- to 2.84- fold after introducing ionomer highlights the adverse interaction of Ni to Nafion® ionomer. It has been reported that metal ion contamination reduces the O_2 permeability within the ionomer coated Pt electrodes [37]. Braaten et al attributed this effect to cross-linking induced between the sulfonate groups of ionomer decreasing the water content in the ionomer layer [39].

To further understand the catalyst/ionomer interaction within the NW array GDEs, the cell temperature was increased to a high temperature of 50°C as close as possible to that in PEMFCs (i.e. 80°C). 50°C is used here because a higher temperature generates bubbles in liquid electrolyte thus affecting the measurement. Similar ECSAs were obtained (Table S1), however; there were key changes in the kinetic region of the LSVs (Figure 7b and c). Figure 7d compares the mass activities at 0.9 V vs. RHE of all GDEs at 25 and 50°C. Compared to 25°C, the mass activity of the Pt NW array GDE increased by 2.28 and 1.70 fold to 1.89 and 8.65 mA mg_{Pt}^{-1} for the plain and ionomer coated GDE, respectively. However, this is only 1.17-fold (3.97 mA mg_{Pt}^{-1}) for the plain PtNi NW array GDE, and even reduces from 14.44 to 13.93 mA mg_{Pt}^{-1} for the ionomer coated PtNi NW array GDE which is only 1.61-fold over that of the ionomer coated Pt NW array GDE. The lower enhancement value for PtNi (cf. Pt) can be ascribed to Ni loss which results in a reduction in the inherent activity of the surface. A crossover between both LSVs for the plain and ionomer coated PtNi NW array GDEs further indicates that the Ni-ionomer interaction is limiting kinetic activity at the high potential region. While gas permeability through the ionomer layer is a critical issue with regards to mass transport losses at a large current density, the activity recorded at 0.9 V should be little affected by such issues, especially in the idealised GDE environment. However, these results suggest otherwise where probable differences in the diffusivity of O_2 through the

ionomer are significant enough to change measured activities at 0.9 V vs. RHE. It is therefore proposed that the unfavourable ionomer contamination is significantly accelerated at a high temperature (e.g. 50°C here or 80°C in PEMFCs) compared to that at 25°C which is the temperature usually used in half-cell measurement. This is the leading cause for the reduced mass activities at high temperature, and also the possible main reason leading to the disparity between ORR catalytic activity measured in half-cell measurement and single cell test environments.

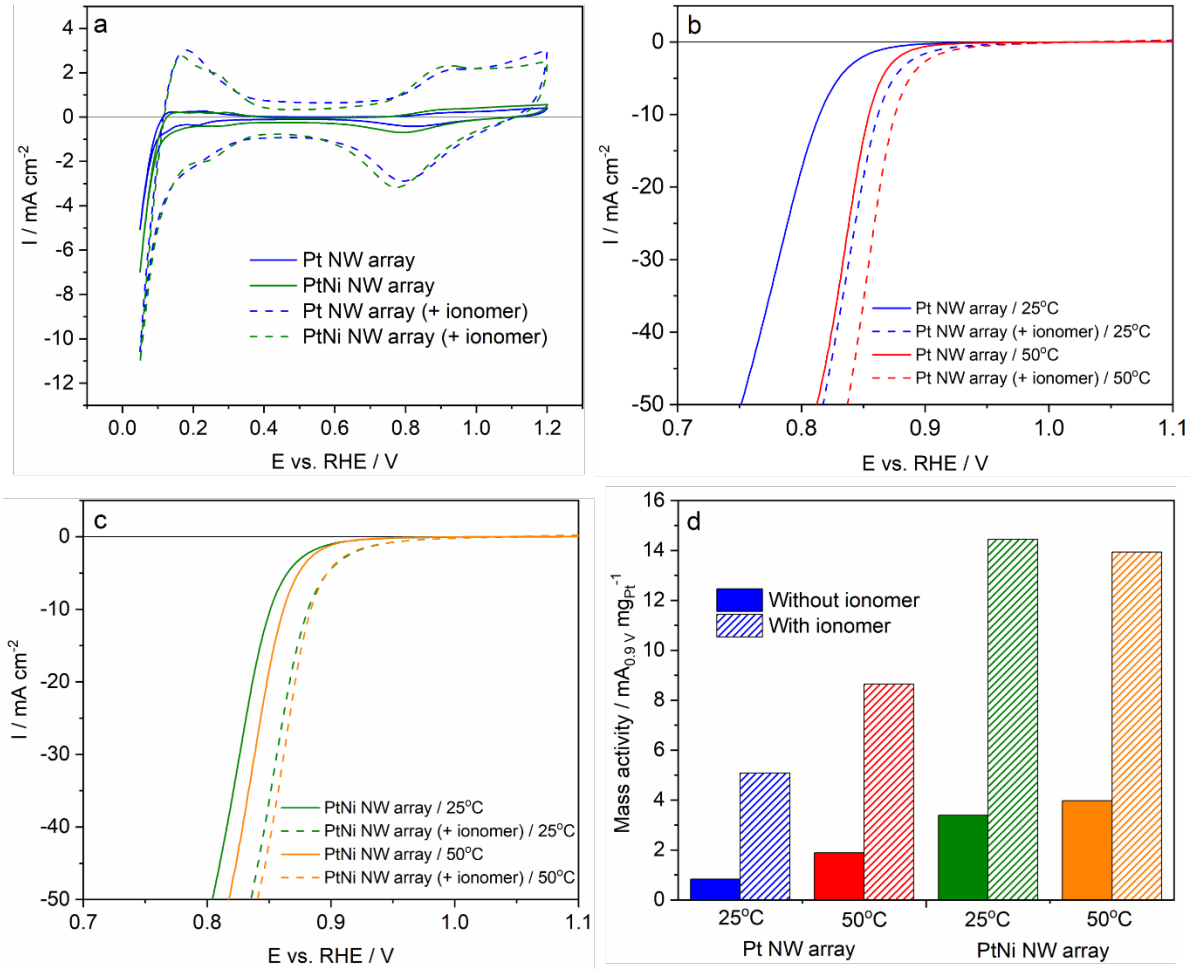

Figure 7: Ex-situ GDE measurement in 0.1 M $HClO_4$ aqueous electrolyte: **(a)** CVs of the GDEs (0.312 mg_{Pt} cm^{-2}) in the potential range 0.05-1.2 V vs. RHE with a scan rate of 20 mV s^{-1} at 25°C

with N_2 gas flow at 0.4 SCFH. LSV plots (corrected with the internal resistance and double layer) in the range 1.2-0.05 V vs. RHE at a scan rate of 10 mV s^{-1} with and without ionomer at 25 and 50°C under a flow of O_2 for **(b)** the Pt NW array and **(c)** PtNi NW array (200°C, AL) GDEs. **(d)** Comparison of the mass activities for all electrodes at 25 and 50°C.

3.3. Single cell performance

For ORR catalyst development, it is critical to understand their real catalytic behaviour in a working PEMFC. For example, catalysts of Pt coated (both galvanic displacement and atomic layer deposition) Ni NWs have been demonstrated with very high ORR catalytic activities by Pivovar and co-workers using half-cell RDE measurement in liquid electrolyte. However, they found that these catalysts showed very limited power performance in fuel cells, in particular the electrode performance severely suffered from Ni dissolution and treatment such as ion exchange or acid leaching was therefore required for the catalysts prior to fabrication into MEAs [33,38,40–43].

Figure 8 shows the polarization curves and (G)EIS plot at a low current density (30 mA cm^{-2}) of the MEAs with PtNi NW array (200°C) and PtNi NW array (200°C, AL) cathodes. Figure S7 shows the P(EIS) at the intermediate and high current density regions. Without acid leaching, the PtNi NW array electrode exhibits much lower power performance although a higher OCP and slightly smaller charge transfer resistance in comparison to the acid leached one. The initial drop at about 50 mA cm^{-2} can be attributed to the slightly larger internal resistance (shown with the real impedance at the high frequency region), resulting from the decreased proton conductivity in the PEM [44]. This was also reported in the aforementioned PtNi NW system where Mauger et al ascribed the reason to the blocking of sulfuric acid groups in the PEM [42]. The large drop at the higher current density region is caused by mass transport limitation, indicative of the aforementioned ionomer contamination mechanism. The acid leaching mitigates these effects by removing Ni both on Pt

NW surface and in the carbon paper/MPL interface (Figure 3), but also leading to a slightly larger charger transfer resistance and the kinetic performance is reduced. Jia et al experimentally verified that if the PtM_x ratio is higher than the optimal value for ORR catalytic activity, the catalyst resides on the weak Pt-O binding leg of the famous volcano plot, and thus dissolution leads to a strengthening of the Pt-O bond and thus increased catalytic activity [45]. In this work, the reduction in catalytic performance suggests that the PtNi NW arrays reside on the strong binding leg and so the opposite relation is true.

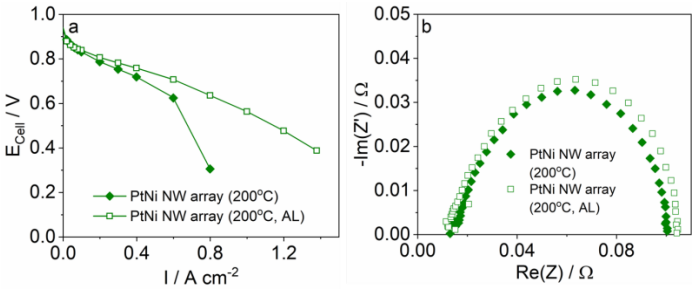

Figure 8: (a) Polarization curves and **(b)** EIS plots at 30 mA cm^{-2} for the PtNi NW array GDEs (annealed at 200°C) before and after the acid leaching (0.312 mg_{Pt} cm^{-2}). Cell temperature 80°C, cathode/anode parameters of: air/H_2 supply, 2.3/2.5 absolute pressure, 1.5/1.3 stoichiometric coefficient, 30%/50% RH, respectively.

To understand the influence of the Ni content on the GDE power performance, precursors with different Ni amounts, Pt_3Ni_2, Pt_3Ni_4 and Pt_3Ni_6 were studied. The polarization curves are shown in Figure S7a and the GDE made from Pt_3Ni_4 exhibits the highest power performance. Our previous study demonstrated that 250°C was the sintering transition temperature for the Pt NW/C catalyst [25] and so with the PtNi NW array GDEs, the annealing temperature was also refined with the optimal condition found at 200°C (Figure S7b). The TEM analysis shows slight morphological changes of the PtNi NW arrays annealed at 250°C, and compared to the annealing at 150°C, the one at 200°C

benefits from the reduced Ni oxides, enhanced alloying and protection to dissolution. The different surface properties of PtNi NWs over Pt NWs mean a different proton conducting ionomer loading is required for the PtNi NW GDE. The results (Figure S7c) indicate that the PtNi NW GDE with a reduced ionomer loading of 0.4 mg_{Naf} cm^{-2} exhibits the best power performance, as compared to a low loading (i.e. 0.2 mg_{Naf} cm^{-2}) with limited proton transport path and a high loading (i.e. 0.6 mg_{Naf} cm^{-2}) inducing O_2 mass transport limitations. Therefore, the optimal fabrication process for the PtNi NW array GDE can be determined as with the precursor ratio Pt_3Ni_4, annealing temperature of 200°C, acid leached and ionomer loading of 0.4 mg_{Naf} cm^{-2}. For simplification in the following discussion, these conditions are denoted as PtNi NW array* GDE.

Figure 9a compares the polarization and power density curves of a Pt/C benchmark catalyst (0.41 mg_{Pt} cm^{-2} [26]), Pt NW array and PtNi NW array* cathodes. A power density trend of PtNi NW array* > Pt NW array > Pt/C is found with the value of 0.541, 0.504 and 0.442 W cm^{-2} at 0.6 V, respectively. To help understand the power performance difference, the ECSA was approximated for each GDE using the H_{des} region of CVs conducted under a cathode flow of N_2(Figure 9b)[8]. For the Pt/C, Pt NW array and PtNi NW array* cathodes, ECSAs are 40.1, 21.8 and 21.4 m^2 g_{Pt}^{-1}, respectively. The similarity to the values obtained in the ex-situ GDE measurement suggests an excellent mechanical reliability of the NW array catalyst structure within the GDE and it is well kept in the hot pressing in making the MEAs. The lower ECSAs of the NW array systems are due to the lower surface to bulk ratio of 1D morphologies and is consistent with previous studies [23]. Even with the lower ECSAs, enhanced single cell performances are recorded for the NW array GDEs. Furthermore, the PtNi NW array* GDE shows slightly higher power density over the Pt NW array GDE with a very similar ECSA, indicating the positive contribution of Ni.

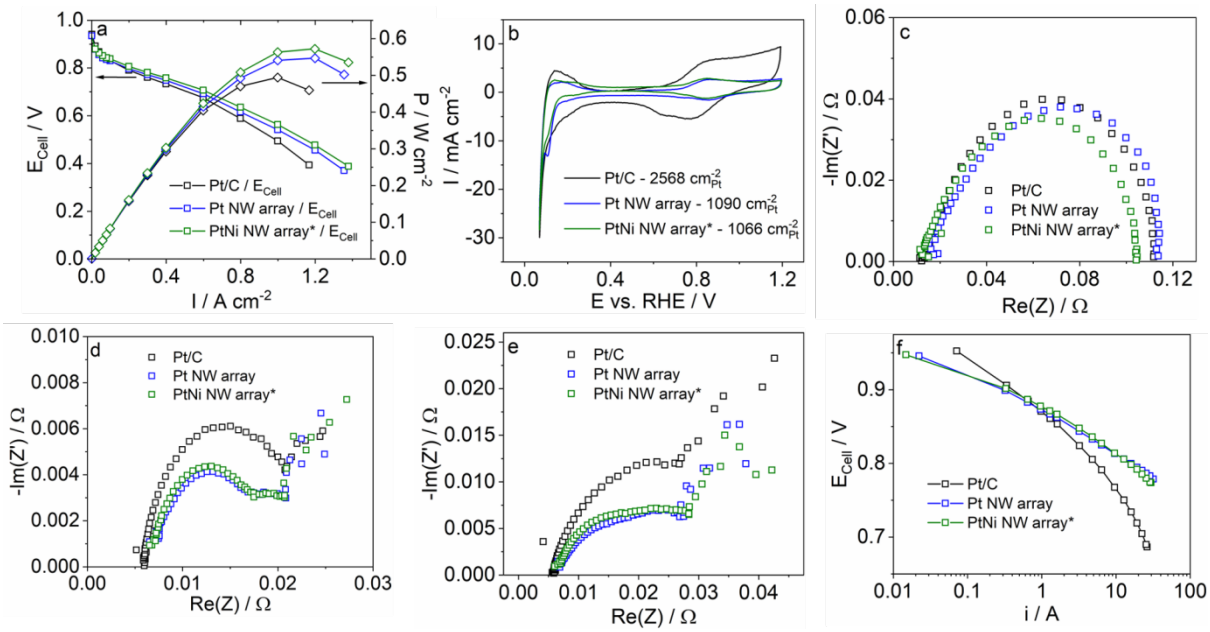

Figure 9: Comparison of power performance for the Pt/C (0.41 mg_{Pt} cm^{-2}), Pt NW array and PtNi NW array* GDEs (0.312 mg_{Pt} cm^{-2}): **(a)** polarization curves; **(b)** cathode CVs with a scan rate of 20 mV s^{-1} and N_2 at the cathode; EIS plots at **(c)** 30 mA cm^{-2}, **(d)** 0.65 V and **(e)** 0.5 V; and **(f)** Tafel plots after the internal resistance and H_2 crossover correction (cathode/anode conditions of: O_2/H_2 supply, 1.5/1.5 bar absolute pressure, 9.5/2 stoichiometric coefficient and 100 %/100 % RH).

To further elucidate the performance enhancements, EIS analysis was conducted and the spectra are shown in Figure 9c-9e. At the low current density at 30 mA cm^{-2} (Figure 9c), very similar charge transfer resistances (R_{CT}) are found for the Pt NW array and Pt/C GDEs. A reduced slope in the mid-high frequency regime for the Pt NW arrays in comparison to Pt/C indicates a larger ionic resistivity as a result of sub-optimal ionomer-NW contact [46,47]. The PtNi NW array* GDE shows a similar slope to the Pt/C GDE suggesting improved proton transport because of the better ionomer-catalyst contact resulting from the higher hydrophilicity PtNi NWs (*cf.* Pt NWs) [48]. Furthermore, a smaller R_{CT} confirms the improved ORR catalytic activity. For EIS spectra at the high current

densities/low cell potentials (Figures 9d and 9e), impedances are both equally smaller than that of Pt/C indicating higher reaction rates and improved mass transfer with the NW GDEs.

Polarization curves were also conducted under O_2 atmosphere at the cathode to minimize the influence of mass transport losses for a better understanding of the ORR catalytic activity in MEA operation [28]. The curves were corrected for both internal resistance and H_2 crossover, resulting in Tafel plots presented in Figure 9f. The mass activity obtained increases modestly from 0.060 $A_{0.9V}$ mg_{Pt}^{-1} for the Pt/C GDE to 0.062 and 0.070 $A_{0.9V}$ mg_{Pt}^{-1} for the Pt NW array and PtNi NW arrays* GDEs, respectively (Table S2). Suggesting an inherent ORR catalytic activity order of PtNi NW array* > Pt NW array > Pt/C is the respective specific activities of 326, 285 and 154 $\mu A_{0.9V}$ cm_{Pt}^{-2}. These enhancements are thought to be due to the high aspect ratio of crystalline facets in the NWs as well as lattice-strain effects additionally presented in the PtNi NW arrays, as supported by previously published data recorded in half-cell measurement using the rotating disk electrode method [16,25]. The Tafel plots also demonstrate a larger absolute current for the Pt/C GDE in the region above 0.9 V in comparison to the NW array GDEs (in the 16 cm^2 MEA), and this can be ascribed to the much larger ECSA presented. Reductions in Tafel slope are also observed for the Pt NW array (44 mV dec^{-1}) and PtNi NW array* (38 mV dec^{-1}) GDEs in comparison to the Pt/C GDE (69 mV dec^{-1}) indicating a possible fast catalytic reaction mechanism for the ORR in the kinetic region [49] and the contribution from the thin nanowire CLs [8,24,50].

3.4. Accelerated degradation testing in PEMFC single cells

To evaluate the durability of the as-prepared GDEs, ADT was conducted by potential cycling for 3000 cycles between 0.6 - 1.2 V vs. RHE at a scan rate of 100 mV s^{-1} with the cathode fed with N_2. Figure 10a shows the ECSA loss of 76% and 51% for the Pt/C and Pt NW array GDEs,

respectively. The better stability of Pt NWs is consistent with previous studies showing 1D Pt nanostructures have a higher tolerance to the catalyst degradation mechanisms such as dissolution, Oswald ripening and aggregation [16,51]. After the introduction of Ni, the PtNi NW array* GDE exhibits a higher ECSA loss of 60% (*cf.* 51% of the Pt NW array GDE). After the ADT the power densities for Pt/C, Pt NW array and PtNi NW array GDEs are 0.308, 0.393 and 0.390 W cm^{-2} at 0.6 V, respectively, corresponding to losses of 30, 22 and 28% to the initial power densities. The major factor for the degradation is the loss of the ECSA, but for the PtNi NW array* GDE the ionomer contamination and specific activity loss through Ni dissolution are also compounding issues. Relative loss of specific activity for the PtNi NWs in comparison to the pure Pt NWs was found during analysis of the performance under O_2 atmosphere where similar activities of 596 and 598 $\mu A\ cm_{Pt}^{-2}$, respectively, were recorded after ADT, suggesting near identical final intrinsic catalytic activity. An increase in specific activity with respect to the pre-ADT GDEs is attributable to particle size effects associated with particle size increases from the extended voltage cycling and was also found for the Pt/C (TKK) GDE. Nevertheless, these results show that both NW array GDEs show enhanced durability to power performance loss than the Pt/C GDE, and that the performance enhancements afforded by impregnated Ni are mitigated during extended tests.

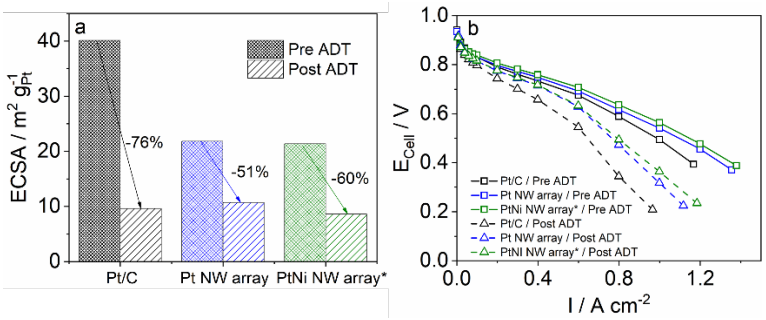

Figure 10: Comparison of the (a) ECSAs and (b) polarization curves before and after the ADT (3000 potential sweeping cycles between 0.6 - 1.2 V vs. RHE at a scan rate of 100 mV s^{-1}) for the Pt/C (0.41 mg_{Pt} cm^{-2}), Pt NW array and PtNi NW array* GDEs (0.312 mg_{Pt} cm^{-2}).

4. Conclusions

PtNi NW array GDEs are fabricated by an impregnation/annealing method. Cross sectional SEM and ICP-MS analyses indicate that Ni primarily deposits at the carbon fibre substrate/MPL interface within the GDL. This deposition results in the ionomer contamination and ion exchange in PEM which significantly reduces the power performance of the GDEs. The acid leaching partially mitigates the negative effect and Ni is left only in the NW structures. The PtNi NW array GDE with the optimal annealing temperature of 200°C, acid leached and Nafion® ionomer content of 0.4 mg cm^{-2}, demonstrates 1.07- and 1.22-fold increases in power density in comparison to the Pt NW array and Pt/C GDEs, respectively. The ex-situ GDE measurement in 0.1 M $HClO_4$ aqueous electrolyte at 25°C records a 2.84-fold enhancement in the mass catalytic activity for the PtNi NW array GDE as compared to the Pt NW array GDE. However, at the elevated temperature of 50°C, the enhancement decreases to 1.61-fold, and the introduction of ionomer in the PtNi NW array GDE even results in a decreased mass activity, which are ascribed to the leaching of Ni and the Ni ion contamination to the ionomer at the high temperature, further limiting the power performance improvement in operating fuel cells. In addition, the leaching of Ni and ionomer contamination result in worse durability of the PtNi NW array GDE finally leading to a similar end power density to the Pt NW array GDE after the ADT. The ionomer coating is concluded to have a drastic negative impact on the PtNi catalytic activities in operating fuel cell environment thus highlighting the potential of ionomer free CLs for utilising PtNi alloy catalysts in PEMFCs.

ASSOCIATED CONTENT

Supporting Information. Contains supporting SEM, SEM-EDX, XRD, XPS, ex-situ GDE and single cell testing data (1 file .docx)

AUTHOR INFORMATION

Corresponding Author

*Corresponding author, Tel: +44 121 4158696

E-mail address: s.du@bham.ac.uk (S. Du)

Present Addresses

†Peter Mardle: School of Chemistry, Simon Fraser University, Burnaby, BC, V5A 1S6, Canada.

Author Contributions

All authors have given approval to the final version of the manuscript.

Funding Sources

P. Mardle is funded by the EPSRC Centre for Doctoral Training in Fuel Cells and their Fuels (EP/L015749/1).

ACKNOWLEDGEMENTS

XPS data collection was performed at the EPSRC National Facility for XPS (HarwellXPS) operated by Cardiff University and UCL, under contract No. PR16195. SEM and TEM were conducted at the Centre for Electron Microscopy, University of Birmingham. Acknowledgement is also due to Dr David Morgan from HarwellXPS for his comments on XPS fitting.

ABBREVIATIONS

1D, one-dimensional; AL, acid leached; ASP, active screen plasma; AST, accelerated stability test; CL, catalyst layer; CV, cyclic voltammetry; ECSA, electrochemical surface area; EDX, energy dispersive X-ray; GDE, gas diffusion electrode; GDL, gas diffusion layer; (G)EIS, galvano-electrochemical impedance spectroscopy; H_{des}, hydrogen desorption; ICP-MS, inductively coupled plasma mass spectrometry; JM, Johnson Matthey; LSV, linear sweep voltammetry; MEA, membrane electrode assembly; MPL, microporous layer; NP, nanoparticle; NW, nanowire; OCP, open circuit potential; ORR, oxygen reduction reaction; (P)EIS, potentio-electrochemical impedance spectroscopy; PEMFC, proton exchange membrane fuel cell; PGM, platinum group metal; PTFE, polytetrafluoroethylene; R_{CT}, charge transfer resistance; RDE, rotating disk electrode; RHE, reference hydrogen electrode; SEM, scanning electron microscopy; STEM, scanning transmission electron microscopy; TEM, transmission electron microscopy; TKK, Tanaka KikinzokuKogyo K. K.; XPS, X-ray photoelectron spectroscopy; XRD, X-ray diffraction.

REFERENCES

(1) Papageorgopoulos, D. "Fuel Cell R&D Overview." In *2019 Annual Merit Review and Peer Evaluation Meeting*; US DoE - Fuel Cells Technologies Office, 2019.

(2) Wilson, M. S.; Gottesfeld, S. Thin-Film Catalyst Layers for Polymer Electrolyte Fuel Cell Electrodes. *J. Appl. Electrochem.* **1992**, *22* (1), 1–7. https://doi.org/10.1007/BF01093004.

(3) Shao, M.; Chang, Q.; Dodelet, J.-P.; Chenitz, R. Recent Advances in Electrocatalysts for Oxygen Reduction Reaction. *Chem. Rev.* **2016**, *116* (6), 3594–3657. https://doi.org/10.1021/acs.chemrev.5b00462.

(4) Nie, Y.; Li, L.; Wei, Z. Recent Advancements in Pt and Pt-Free Catalysts for Oxygen Reduction Reaction. *Chem. Soc. Rev.* **2015**, *44* (8), 2168–2201. https://doi.org/10.1039/C4CS00484A.

(5) Sui, S.; Wang, X.; Zhou, X.; Su, Y.; Riffat, S.; Liu, C. jun. A Comprehensive Review of Pt Electrocatalysts for the Oxygen Reduction Reaction: Nanostructure, Activity, Mechanism and Carbon Support in PEM Fuel Cells. *J. Mater. Chem. A* **2017**, *5* (5), 1808–1825. https://doi.org/10.1039/C6TA08580F.

(6) Li, M.; Li, M.; Zhao, Z.; Cheng, T.; Fortunelli, A.; Chen, C.; Yu, R.; Gu, L.; Merinov, B.; Lin, Z.; et al. Ultrafine Jagged Platinum Nanowires Enable Ultrahigh Mass Activity for the Oxygen Reduction Reaction. *Science* **2016**, *9050* (November), 1414–1419. https://doi.org/10.1126/science.aaf9050.

(7) Kongkanand, A.; Mathias, M. F. The Priority and Challenge of High-Power Performance of Low-Platinum Proton-Exchange Membrane Fuel Cells. *J. Phys. Chem. Lett.* **2016**, *7* (7), 1127–1137. https://doi.org/10.1021/acs.jpclett.6b00216.

(8) Gasteiger, H. A.; Panels, J. E.; Yan, S. G. Dependence of PEM Fuel Cell Performance on Catalyst Loading. **2004**, *127*, 162–171. https://doi.org/10.1016/j.jpowsour.2003.09.013.

(9) Stephens, I. E. L.; Rossmeisl, J.; Chorkendorff, I. Toward Sustainable Fuel Cells. *Science* **2016**, *354* (6318), 1378–1380. https://doi.org/10.1126/science.aal3303.

(10) Wang, M.; Zhang, H.; Thirunavukkarasu, G.; Salam, I.; Varcoe, J. R.; Mardle, P.; Li, X.; Mu, S.; Du, S. Ionic Liquid-Modified Microporous ZnCoNC-Based Electrocatalysts for Polymer Electrolyte Fuel Cells. *ACS Energy Lett.* **2019**, *4* (9). https://doi.org/10.1021/acsenergylett.9b01407.

(11) Pan, L.; Ott, S.; Dionigi, F.; Strasser, P. Current Challenges Related to the Deployment of Shape-Controlled Pt Alloy Oxygen Reduction Reaction Nanocatalysts into Low Pt-Loaded Cathode Layers of Proton Exchange Membrane Fuel Cells. *Curr. Opin. Electrochem.* **2019**, *18*, 61–71. https://doi.org/10.1016/j.coelec.2019.10.011.

(12) Du, S. Pt-Based Nanowires as Electrocatalysts in Proton Exchange Fuel Cells. *Int. J. Low-Carbon Technol.* **2012**, *7* (1), 44–54. https://doi.org/10.1093/ijlct/ctr027.

(13) Bu, L.; Ding, J.; Guo, S.; Zhang, X.; Su, D.; Zhu, X.; Yao, J.; Guo, J.; Lu, G.; Huang, X. A

General Method for Multimetallic Platinum Alloy Nanowires as Highly Active and Stable Oxygen Reduction Catalysts. *Adv. Mater.* **2015**, *27* (44), 7204–7212. https://doi.org/10.1002/adma.201502725.

(14) Bu, L.; Zhang, X.; Shen, X.; Su, D.; Lu, G.; Zhu, X.; Yao, J.; Guo, J.; Guo, S.; Huang, X. Surface Engineering of Hierarchical Platinum-Cobalt Nanowires for Efficient Electrocatalysis. *Nat. Commun.* **2016**, *7*, 1–10. https://doi.org/10.1038/ncomms11850.

(15) Jiang, K.; Zhao, D.; Guo, S.; Zhang, X.; Zhu, X.; Guo, J.; Lu, G.; Huang, X. Efficient Oxygen Reduction Catalysis by Subnanometer Pt Alloy Nanowires. *Sci. Adv.* **2017**, *3* (2), 1–8. https://doi.org/10.1126/sciadv.1601705.

(16) Sun, S.; Zhang, G.; Geng, D.; Chen, Y.; Li, R.; Cai, M.; Sun, X. A Highly Durable Platinum Nanocatalyst for Proton Exchange Membrane Fuel Cells: Multiarmed Starlike Nanowire Single Crystal. *Angew. Chemie - Int. Ed.* **2011**, *50* (2), 422–426. https://doi.org/10.1002/anie.201004631.

(17) Meng, H.; Zhan, Y.; Zeng, D.; Zhang, X.; Zhang, G.; Jaouen, F. Factors Influencing the Growth of Pt Nanowires via Chemical Self-Assembly and Their Fuel Cell Performance. *Small* **2015**, *11* (27), 3377–3386. https://doi.org/10.1002/smll.201402904.

(18) Sun, S.; Yang, D.; Villers, D.; Zhang, G.; Sacher, E.; Dodelet, J. P. Template- And Surfactant-Free Room Temperature Synthesis of Self-Assembled 3D Pt Nanoflowers from Single-Crystal Nanowires. *Adv. Mater.* **2008**, *20* (3), 571–574. https://doi.org/10.1002/adma.200701408.

(19) Sun, S.; Jaouen, F.; Dodelet, J. P. Controlled Growth of Pt Nanowires on Carbon Nanospheres and Their Enhanced Performance as Electrocatalysts in PEM Fuel Cells. *Adv. Mater.* **2008**, *20* (20), 3900–3904. https://doi.org/10.1002/adma.200800491.

(20) Du, S. A Facile Route for Polymer Electrolyte Membrane Fuel Cell Electrodes with in Situ Grown Pt Nanowires. *J. Power Sources* **2010**, *195* (1), 289–292. https://doi.org/10.1016/j.jpowsour.2009.06.091.

(21) Lu, Y.; Du, S.; Steinberger-Wilckens, R. Three-Dimensional Catalyst Electrodes Based on PtPd Nanodendrites for Oxygen Reduction Reaction in PEFC Applications. *Appl. Catal. B Environ.* **2016**, *187*, 108–114. https://doi.org/10.1016/j.apcatb.2016.01.019.

(22) Sui, S.; Wei, Z.; Su, K.; He, A.; Wang, X.; Su, Y.; Hou, X.; Raffet, S.; Du, S. Pt Nanowire Growth Induced by Pt Nanoparticles in Application of the Cathodes for Polymer Electrolyte Membrane Fuel Cells (PEMFCs). *Int. J. Hydrogen Energy* **2018**, *43*, 20041–20049. https://doi.org/10.1016/j.ijhydene.2018.09.009.

(23) Du, S.; Lin, K.; Malladi, S. K.; Lu, Y.; Sun, S.; Xu, Q.; Steinberger-Wilckens, R.; Dong, H. Plasma Nitriding Induced Growth of Pt-Nanowire Arrays as High Performance Electrocatalysts for Fuel Cells. *Sci. Rep.* **2014**, *4 : 6439*, 1–6. https://doi.org/10.1038/srep06439.

(24) Lu, Y.; Du, S.; Steinberger-Wilckens, R. Temperature-Controlled Growth of Single-Crystal Pt Nanowire Arrays for High Performance Catalyst Electrodes in Polymer Electrolyte Fuel Cells. *Appl. Catal. B Environ.* **2015**, *164*, 389–395. https://doi.org/10.1016/j.apcatb.2014.09.040.

(25) Mardle, P.; Du, S. Annealing Behaviour of Pt and PtNi Nanowires for Proton Exchange Membrane Fuel Cells. *Materials* **2018**, *11*, 1473–1485. https://doi.org/10.3390/ma11081473.

(26) Mardle, P.; Ji, X.; Wu, J.; Guan, S.; Dong, H.; Du, S. Thin Film Electrodes from Pt Nanorods Supported on Aligned N-CNTs for Proton Exchange Membrane Fuel Cells. *Appl. Catal. B Environ.* **2020**, *260* (March 2019), 118031–118038. https://doi.org/10.1016/j.apcatb.2019.118031.

(27) Tsotridis, G.; Pilenga, A.; Marco, G. De; Malkow, T. *EU Harmonised Test Protocols for PEMFC MEA Testing in Single Cell Configuration for Automotive Applications; JRC Science for Policy Report*; 2015. https://doi.org/10.2790/54653.

(28) *Multi-Year Research, Development, and Demonstration Plan: 3.4 Fuel Cells*; US Department of Energy (DOE), 2017.

(29) Gasteiger, H. A.; Kocha, S. S.; Sompalli, B.; Wagner, F. T. Activity Benchmarks and Requirements for Pt, Pt-Alloy, and Non-Pt Oxygen Reduction Catalysts for PEMFCs. *Appl. Catal. B Environ.* **2005**, *56* (1-2 SPEC. ISS.), 9–35. https://doi.org/10.1016/j.apcatb.2004.06.021.

(30) Garsany, Y.; Baturina, O. a; Swider-Lyons, K. E.; Kocha, S. S. Experimental Methods for Quantifying the Activity of Platinum Electrocatalysts for the Oxygen Reduction Reaction. *Anal. Chem.* **2010**, *82* (15), 6321–6328. https://doi.org/10.1021/ac100306c.

(31) Elvington, M. C.; Colón-Mercado, H. R. Pt and Pt/Ni "Needle" Eletrocatalysts on Carbon Nanotubes with High Activity for the ORR. *Electrochem. Solid-State Lett.* **2012**, *15* (2), K19–K22. https://doi.org/10.1149/2.022202esl.

(32) Du, S.; Lu, Y.; Steinberger-Wilckens, R. PtPd Nanowire Arrays Supported on Reduced Graphene Oxide as Advanced Electrocatalysts for Methanol Oxidation. *Carbon N. Y.* **2014**, *79* (1), 346–355. https://doi.org/10.1016/j.carbon.2014.07.076.

(33) Alia, S. M.; Ngo, C.; Shulda, S.; Ha, M.-A.; Dameron, A. A.; Weker, J. N.; Neyerlin, K. C.; Kocha, S. S.; Pylypenko, S.; Pivovar, B. S. Exceptional Oxygen Reduction Reaction Activity and Durability of Platinum–Nickel Nanowires through Synthesis and Post-Treatment Optimization. *ACS Omega* **2017**, *2* (4), 1408–1418. https://doi.org/10.1021/acsomega.7b00054.

(34) Ren, W.; Li, D.; Liu, H.; Mi, R.; Zhang, Y.; Dong, L.; Dong, L. Lithium Storage Performance of Carbon Nanotubes with Different Nitrogen Contents as Anodes in Lithium Ions Batteries. *Electrochim. Acta* **2013**, *105*, 75–82. https://doi.org/10.1016/j.electacta.2013.04.145.

(35) Wang, C.; Chi, M.; Li, D.; Strmcnik, D.; Van Der Vliet, D.; Wang, G.; Komanicky, V.; Chang, K. C.; Paulikas, A. P.; Tripkovic, D.; et al. Design and Synthesis of Bimetallic Electrocatalyst with Multilayered Pt-Skin Surfaces. *J. Am. Chem. Soc.* **2011**, *133* (36), 14396–14403. https://doi.org/10.1021/ja2047655.

(36) Antolini, E.; Salgado, J. R. C.; dos Santos, a. M.; Gonzalez, E. R. Carbon-Supported Pt-Ni

Alloys Prepared by the Borohydride Method as Electrocatalysts for DMFCs. *Electrochem. Solid-State Lett.* **2005**, *8* (4), A226–A230. https://doi.org/10.1149/1.1870632.

(37) Okada, T.; Dale, J.; Ayato, Y.; Asbjørnsen, O. A.; Yuasa, M.; Sekine, I. Unprecedented Effect of Impurity Cations on the Oxygen Perfluorinated Ionomer. *Langmuir* **1999**, *15*, 8490–8496. https://doi.org/10.1021/la990625e.

(38) Alia, S. M.; Pylypenko, S.; Dameron, A.; Neyerlin, K. C.; Kocha, S. S.; Pivovar, B. S. Oxidation of Platinum Nickel Nanowires to Improve Durability of Oxygen-Reducing Electrocatalysts. *J. Electrochem. Soc.* **2016**, *163* (3), F296–F301. https://doi.org/10.1149/2.0081605jes.

(39) Braaten, J.; Kongkanand, A.; Litster, S. Oxygen Transport Effects of Cobalt Cation Contamination of Ionomer Thin Films in Proton Exchange Membrane Fuel Cells. *ECS Trans.* **2017**, *80* (8), 283–290. https://doi.org/10.1149/08008.0283ecst.

(40) Alia, S. M.; Larsen, B. A.; Pylypenko, S.; Cullen, D. A.; Diercks, D. R.; Neyerlin, K. C.; Kocha, S. S.; Pivovar, B. S. Platinum-Coated Nickel Nanowires as Oxygen-Reducing Electrocatalysts. *ACS Catal.* **2014**, *4* (4), 1114–1119. https://doi.org/10.1021/cs401081w.

(41) McNeary, W. W.; Ngo, C.; Linico, A. E.; Zack, J. W.; Roman, A. M.; Hurst, K. M.; Alia, S. M.; Medlin, J. W.; Pylypenko, S.; Pivovar, B. S.; et al. Extended Thin-Film Electrocatalyst Structures via Pt Atomic Layer Deposition. *ACS Appl. Nano Mater.* **2018**, *1* (11), 6150–6158. https://doi.org/10.1021/acsanm.8b01369.

(42) Mauger, S. A.; Neyerlin, K. C.; Alia, S. M.; Ngo, C.; Babu, S. K.; Hurst, K. E.; Pylypenko, S.; Litster, S.; Pivovar, B. S. Fuel Cell Performance Implications of Membrane Electrode Assembly Fabrication with Platinum-Nickel Nanowire Catalysts. *J. Electrochem. Soc.* **2018**, *165* (3), F238–F245. https://doi.org/10.1149/2.1061803jes.

(43) Shulda, S.; Weker, J. N.; Ngo, C.; Alia, S. M.; Mauger, S. A.; Neyerlin, K. C.; Pivovar, B. S.; Pylypenko, S. 2D and 3D Characterization of PtNi Nanowire Electrode Composition and Structure. *ACS Appl. Nano Mater.* **2019**, *2* (1), 525–534. https://doi.org/10.1021/acsanm.8b02097.

(44) Dicks, A.; Larminie, J. *"Fuel Cell Systems Explained";* Wiley, 2003.

(45) Jia, Q.; Li, J.; Caldwell, K.; Ramaker, D. E.; Ziegelbauer, J. M.; Kukreja, R. S.; Kongkanand, A.; Mukerjee, S. Circumventing Metal Dissolution Induced Degradation of Pt-Alloy Catalysts in Proton Exchange Membrane Fuel Cells : Revealing the Asymmetric Volcano Nature of Redox Catalysis. *ACS Appl. Nano Mater.* **2016**, *6*, 928–938. https://doi.org/10.1021/acscatal.5b02750.

(46) Du, S.; Millington, B.; Pollet, B. G. The Effect of Nafion Ionomer Loading Coated on Gas Diffusion Electrodes with In-Situ Grown Pt Nanowires and Their Durability in Proton Exchange Membrane Fuel Cells. *Int. J. Hydrogen Energy* **2011**, *36* (7), 4386–4393. https://doi.org/10.1016/j.ijhydene.2011.01.014.

(47) Easton, E. B.; Pickup, P. G. An Electrochemical Impedance Spectroscopy Study of Fuel Cell Electrodes. *Electrochim. Acta* **2005**, *50* (12), 2469–2474. https://doi.org/10.1016/j.electacta.2004.10.074.

(48) Liu, J.; Zenyuk, I. V. Proton Transport in Ionomer-Free Regions of Polymer Electrolyte Fuel Cells and Implications for Oxygen Reduction Reaction. *Curr. Opin. Electrochem.* **2018**, *12*, 202–208. https://doi.org/10.1016/j.coelec.2018.11.015.

(49) Shinagawa, T.; Garcia-esparza, A. T.; Takanabe, K. Insight on Tafel Slopes from a Microkinetic Analysis of Aqueous Electrocatalysis for Energy Conversion. *Nat. Publ. Gr.* **2015**, *5*, 13801. https://doi.org/10.1038/srep13801.

(50) Sleightholme, A. E. S.; Wilkinson, D. P.; Bizzotto, D.; Ye, S.; Gyenge, E. L. Nafion Film-Templated Platinum Electrodes for Oxygen Reduction. *Electrocatalysis* **2010**, *1*, 22–27. https://doi.org/10.1007/s12678-010-0006-1.

(51) Li, B.; Higgins, D. C.; Xiao, Q.; Yang, D.; Zhng, C.; Cai, M.; Chen, Z.; Ma, J. The Durability of Carbon Supported Pt Nanowire as Novel Cathode Catalyst for a 1.5 KW PEMFC Stack. *Appl. Catal. B Environ.* **2015**, *162*, 133–140. https://doi.org/10.1016/j.apcatb.2014.06.040.